

### NUMERICAL CALCULATION OF INTERNAL FLOW INSIDE A HYDRAULIC TURBINE UNDER DIFFERENT OPERATING CONDITIONS

Ji-Wei Shen<sup>1\*</sup>, Qing-Ming Jin<sup>2</sup>, Bo Wang<sup>1</sup>, He-Chao Guo<sup>1</sup>, Fu-Yi Zhang<sup>1</sup> and Ke-Xin Xie<sup>1</sup>

<sup>1</sup>College of Mechanical Engineering, Quzhou University, Quzhou, 324000, China.

<sup>2</sup>Wenzhou Bingyuan Intelligent Technology Co., Ltd., Wenzhou 325800, China.

Article Received on 07/11/2024

Article Revised on 27/11/2024

Article Accepted on 17/12/2024



\*Corresponding Author

Ji-Wei Shen

College of Mechanical  
Engineering, Quzhou  
University, Quzhou,  
324000, China.

#### ABSTRACT

To reveal the energy conversion characteristics of centrifugal pumps being operated as a hydraulic turbine under different flow rates. Based on the STMPLEC algorithm, a numerical simulation of internal viscous flow was conducted for the operation process of a single-stage centrifugal pump as a hydraulic turbine. Through numerical calculations, the hydraulic losses at various components where liquid flows through during the operation of the single-stage centrifugal pump, as well as the evolution characteristics of the internal flow field

in the hydraulic turbine, were obtained. The study focused on analyzing the changes in hydraulic loss for key components such as the impeller, volute, draft tube, and the extension section at the turbine inlet under different flow rates. The research results indicate that the impeller and volute are the main components where hydraulic losses occur within the turbine. The hydraulic loss in the impeller decreases initially and then increases with rising flow rates, while the hydraulic loss in the volute steadily increases. In conclusion, the contours analysis of the flow field inside the turbine indicates that under low flow conditions, the flow within the impeller is relatively uniform. Under design flow conditions, there are vortices at both the inlet and outlet ends of the impeller, with recirculation occurring at the blade outlet. At high flow rates, the range of these vortices further expands, and the flow becomes increasingly chaotic.

**KEYWORDS:** turbine, flow, numerical simulation.

## 1 INTRODUCTION

In industries such as petrochemicals, refining, and seawater desalination, there is a widespread phenomenon of high-pressure fluids being reduced to low pressure through pressure relief valves or being directly discharged. For example, in hydrocracking and residue hydrogenation units, the liquid phase from hot the high-pressure separator is reduced in pressure before entering the hot low-pressure separator pressure reduction zone, with a typical pressure differential of 11 to 15 MPa. The high-amine content stream from the bottom of the high-pressure hydrogen recycle desulfurization tower is sent to the pressure reduction zone, with a typical pressure differential of 14 to 16 MPa. In the copper washing process of the synthetic ammonia refining section, the waste copper liquid pressure discharged from the bottom of the tower is as high as 12 MPa, and then it is reduced to 0.4 MPa after throttling decompression. In the seawater desalination system, the spent concentrated brine discharged from the membrane device has a pressure as high as 5.5-6.0MPa. If it is discharged directly without energy recovery, it will cause serious energy waste. Currently, utilizing a centrifugal pump in reverse as a hydraulic turbine is a very effective means to recover and utilize liquid pressure energy.

In terms of the parametric impact on the hydraulic performance of hydraulic turbines, both domestic and international efforts have been made extensively in parametric design and influence studies aimed at improving the hydraulic efficiency of hydraulic turbines, and significant research achievements have been obtained. Ashish and Derakhshan rounded off the inner sides of the front and rear shrouds of the hydraulic turbine impeller and the blade inlet separately.<sup>[1,2]</sup> Through experiments, they found that this could effectively reduce hydraulic losses and improve conveying efficiency. At the same time, it was proposed that by modifying the installation angle of the backward-curved blades, hydraulic losses could be reduced by 5-10%.The results showed that as the number of blades increases, the efficiency decreases sharply. At the same time, it was found that a reduction in blade height directly leads to a decrease in hydraulic losses through the impeller, but it does not have a major impact on hydraulic performance. This study provides a good reference for improving the efficiency of axial flow pumps in reverse operation mode. Wen-Guang Li is currently one of the few researchers who have publicly reported on the impact of transport medium characteristics on hydraulic turbine performance.<sup>[3,4]</sup> The study found that The optimal flow

rate and energy consumption of the turbine increase with the increase of viscosity, while hydraulic efficiency shows a decreasing trend. The output shaft power is mainly determined by the liquid density. It also points out that the impact of viscosity on turbine performance is more severe than on pumps. The required cavitation margin of a hydraulic turbine increases with the increase in liquid viscosity, but the extent is relatively small; at the same viscosity, it is only 50% to 80% of the required cavitation margin for a pump. The required NPSH determined by the shaft power drop of 3% criterion is basically consistent with that determined by the hydraulic efficiency drop of 1% criterion.

In summary, the study of typical inflow characteristic parameters on energy conversion mechanism of hydraulic turbine has not been involved in domestic and foreign researches, and the unsteady flow process of getting energy mechanism for hydraulic turbine has not been well revealed. Most researchers have conducted their studies under the design conditions of pumps operating as turbines, whereas in actual operation, turbines often run under off-design conditions. Therefore, it is necessary to study the internal flow characteristics and energy conversion mechanisms of pumps operating as turbines under different working conditions, in order to further grasp their operational rules. With the rapid development of computational fluid dynamics and computer technology, numerical calculation has become an important tool for studying the internal flow characteristics of centrifugal pumps. Based on previous research, this study employs computational fluid dynamics methods to investigate a single-stage cantilevered hydraulic turbine with a specific speed of 23.1. The study investigates the distribution patterns of internal flow fields under varying flow conditions, as well as the evolution characteristics of external properties and changes in hydraulic losses. It aims to explore the relationship between the internal flow field distribution and energy conversion mechanisms within the turbine, providing a reference for optimizing design and operational scheduling of the turbine.

## 2 Physical Model and Method

### 2.1 Computational Model

In this study, the rated parameters of the single-stage cantilevered hydraulic turbine are as follows: Flow rate  $Q=12.5\text{m}^3/\text{h}$ , Head  $H=80.78\text{m}$ , Rotational speed  $n=2900\text{r}/\text{min}$ , Turbine impeller inlet diameter  $D_1=52\text{mm}$ , Impeller outlet diameter  $D_2=242\text{mm}$ , Impeller outer diameter  $D_3=242\text{mm}$ , Number of blades  $Z=5$ , Impeller outlet width  $b_2=4\text{mm}$ , Blade outlet angle  $\beta_1=26^\circ$ , Volute base circle diameter  $D_3=248\text{mm}$ , Blade wrap angle  $\beta_2=155^\circ$ .

## 2.2 Mesh Generation

The computational domain of the single-stage hydraulic turbine is shown in Figure 1.

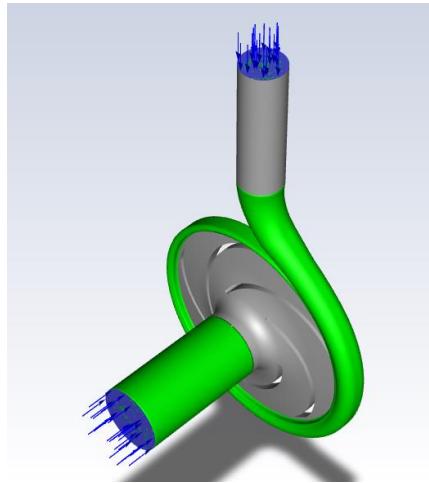


**Figure 1: Computational Domain.**

The total number of cells is 1,032,286. The inlet extension section uses hexahedral meshing with 94,478 cells; the impeller region uses tetrahedral meshing with 533,164 cells; the volute region also uses tetrahedral meshing with 297,788 cells; and the guide vane outlet extension section uses hexahedral meshing with 106,856 cells. During the mesh generation process, we ensured that the quality of all cells was above 0.2.

## 2.3 Control Equations

The computations were carried out using the Fluent platform. Since the liquid flow in the hydraulic turbine is in a turbulent state, this study adopts the RNG k- $\varepsilon$  two-equation model to close the Reynolds-averaged Navier-Stokes equations for describing the liquid flow within the hydraulic turbine. The Multiple Reference Frame (MRF) model is adopted.

$$\frac{\partial}{\partial t}(\rho k) + \frac{\partial}{\partial x_i}(\rho k u_i) = \frac{\partial}{\partial x_j}(\alpha_k \mu_{eff} \frac{\partial k}{\partial x_j}) + G_k + G_b - \rho \varepsilon - Y_M + S_k \quad (1)$$

$$\frac{\partial}{\partial t}(\rho \varepsilon) + \frac{\partial}{\partial x_i}(\rho \varepsilon u_i) = \frac{\partial}{\partial x_j}(\alpha_\varepsilon \mu_{eff} \frac{\partial \varepsilon}{\partial x_j}) + C_{1\varepsilon} \frac{\varepsilon}{k} (G_k + C_{3\varepsilon} G_b) - C_{2\varepsilon} \rho \frac{\varepsilon^2}{k} - R_\varepsilon + S_\varepsilon \quad (2)$$

In the equation:  $\rho$  represents the fluid density,  $C_{1\varepsilon}=1.42$ ,  $C_{2\varepsilon}=1.68$ ,  $G_k$  denotes the generation of turbulent kinetic energy caused by the mean velocity gradient;  $G_b$  is the turbulent kinetic energy produced by buoyancy;  $Y_M$  represents the contribution of fluctuating dilatation in compressible turbulence to the overall dissipation rate;  $\alpha_k$  and  $\alpha_\varepsilon$  are

the reciprocals of the effective Prandtl numbers for  $k$  and  $\epsilon$ , respectively;  $S_k$  and  $S_\epsilon$  are user-defined source terms. This model significantly improves the simulation accuracy of rapid strain flows and vortex flows by introducing additional terms, considering the effects of swirling flows, and addressing swirling motion situations, making it more broadly applicable and reliable in engineering applications.

## 2.4 Calculation Method

The calculations for this study were completed in the professional computational fluid dynamics software package ANSYS-FLUENT. This study only calculates the hydraulic turbine computational domain, so it is necessary to set boundary conditions. The inlet and outlet boundary conditions are pressure inlet (inlet pressure is 8MPa) and velocity inlet, respectively. Considering viscous effects, the wall is set to no-slip with a roughness of 0.5mm, and the convergence condition is that the residual is less than  $10^{-3}$ . To ensure data exchange between the moving and stationary domains, an interface is created at their connection part, to guarantee the normal progress of the simulation. For high Reynolds number flow problems near the wall surface, the standard wall function method is used to avoid directly solving regions with significant viscous effects. The coupling iteration calculation of velocity and pressure terms in the computation is implemented using the SIMPLE algorithm. The computational medium is water at room temperature, with a density  $\rho=998.2\text{kg/m}^3$  and a dynamic viscosity  $\mu=0.001[\text{kg}/(\text{m}\cdot\text{s})]$ , taking gravity into account. In the iterative calculation, all variables employ the default under-relaxation factors. The computation stops and results are read when the calculated residuals meet the requirements and the monitored physical parameters reach stability. By adjusting different inlet flow rates and repeating the calculation process, the characteristic curve of the turbine can be obtained.

## 3 Computational results

### 3.1 External Characteristics

Figure 2 shows the external characteristic curves of the hydraulic turbine under different flow conditions. From the figure, it can be seen that the optimal operating point is at  $Q=197\text{m}^3/\text{h}$ , where the efficiency of the hydraulic turbine reaches its maximum value of 75%. When deviating from the optimal operating point, the turbine has a relatively wide high-efficiency range; for example, at a flow rate of  $Q=275.8\text{m}^3/\text{h}$ , the efficiency is 61%, but there is a significant drop in efficiency at lower flow rates, such as at  $Q=118.2\text{m}^3/\text{h}$ , where the efficiency is only 45%. The power and head of the hydraulic turbine both increase

progressively with the flow rate. When the flow rate is at the optimal operating point of  $Q=197\text{m}^3/\text{h}$ , the power and head are  $p=109\text{kW}$  and  $H=268\text{m}$ , respectively. At low flow rates, the slopes of the external characteristic curves for both power and head are smaller, resulting in a less significant increase. For example, at a flow rate of  $Q=118.2\text{m}^3/\text{h}$ , the power and head are  $p=25\text{kW}$  and  $H=173\text{m}$ , respectively. In contrast, at high flow rates, the slopes of these curves become steeper, indicating a substantial increase. For instance, at a flow rate of  $Q=275.8\text{m}^3/\text{h}$ , the power and head are  $p=242\text{kW}$  and  $H=529\text{m}$ , respectively.

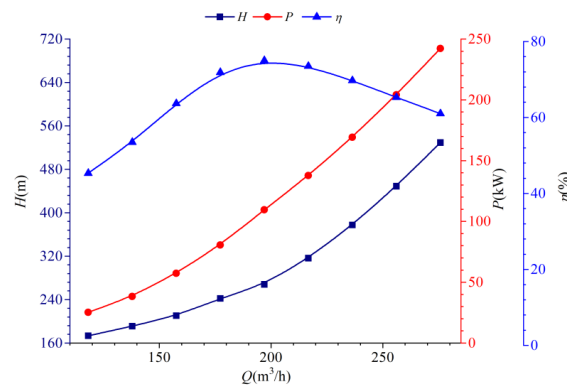


**Figure 2: External Characteristic Curve.**

### 3.2 Hydraulic Loss

Hydraulic loss refers to the pressure loss caused by the viscosity of the medium during the flow process. To compare the hydraulic losses of the hydraulic turbine under different flow conditions, the total hydraulic loss variation curve was calculated based on the law of energy conservation, as shown in Figure 3. It can be observed that the total hydraulic loss initially decreases and then increases. When the flow rate is less than  $140\text{m}^3/\text{h}$ , the total hydraulic loss is slightly higher than the output power. For example, at a flow rate of  $Q=118.2\text{m}^3/\text{h}$ , the total hydraulic loss  $\Delta h=30\text{kW}$ , the input power  $P_{in}=25\text{kW}$ , and the output power  $P_{out}=53\text{kW}$ . The corresponding external characteristic curve indicates that the turbine efficiency is relatively low under low-flow conditions. As the flow rate increases, the output power quickly surpasses the total hydraulic loss, and the slope of the output power curve is much steeper than that of the hydraulic loss curve. At this point, the total hydraulic loss remains relatively stable. The corresponding external characteristic curve shows a significant increase in turbine efficiency. For example, at the design flow rate of  $Q=197\text{m}^3/\text{h}$ , the total hydraulic loss  $\Delta h=33\text{kW}$ , the input power  $P_{in}=136\text{kW}$ , and the output power  $P_{out}=109\text{kW}$ . When the flow rate reaches  $220\text{m}^3/\text{h}$ , the slope of the output power curve remains almost unchanged, while the slope of the total hydraulic loss curve increases rapidly, indicating a gradual decrease in

turbine efficiency under high-flow conditions. For instance, under high-flow conditions such as  $Q=275.8\text{m}^3/\text{h}$ , the total hydraulic loss  $\Delta h=135\text{kW}$ , the input power  $P_{in}=363\text{kW}$ , and the output power  $P_{out}=242\text{kW}$ .

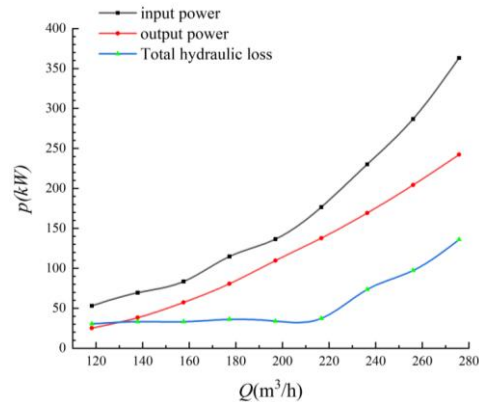
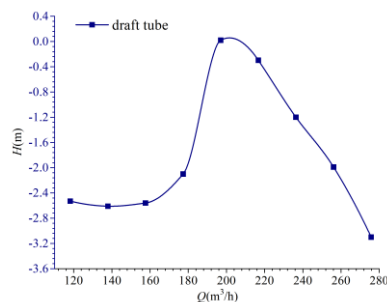
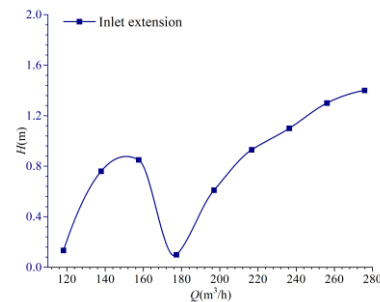


**Figure 3: Variation of input power, output power, and total hydraulic loss with flow rate.**

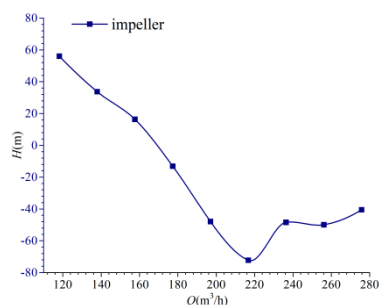
The hydraulic loss regions within the turbine are divided into two main categories: stationary flow regions and moving flow regions. The stationary flow regions include the inlet extension, volute, front and rear cavities, and outlet extension; the moving flow region is the impeller. Figure 4 shows the variation of hydraulic loss with flow rate in various components.



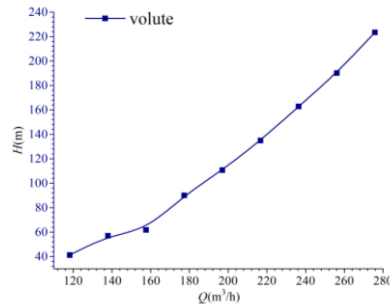
**(a) Hydraulic loss in the draft tube**



**(b) Hydraulic loss in the inlet extension**



**(c) Hydraulic loss in the impeller**



**(d) Hydraulic loss in the volute**

**Figure 4: The variation of hydraulic loss with flow rate in various components.**

It can be seen from Figure 4 (c) that the water power loss curve in the impeller first decreases and then increases with the increase of flow rate. When the inlet and outlet flow rate of the hydraulic turbine reaches  $Q=177.3\text{m}^3/\text{h}$ , the water power loss of the impeller reaches the minimum value of -13 meters, which is slightly less than the designed operating condition. At the design condition flow rate of  $Q=197\text{m}^3/\text{h}$ , the water power loss of the impeller is -47 m. In the low flow rate interval, the curve slope is relatively steep, and the variation range of the water power loss curve inside the impeller is large. When the flow rate exceeds the designed operating condition, the growth rate of the curve slows down. In the simulation, the minimum and maximum flow rates are  $118.2\text{m}^3/\text{h}$  and  $275.8\text{m}^3/\text{h}$  respectively, with corresponding water power losses of the impeller at 56 meters and -40 m. The minimum water power loss in the draft tube is 0.02 meters, occurring at the design flow rate of  $Q=197\text{m}^3/\text{h}$ , indicating relatively low water power loss. The reason for the negative value of hydraulic loss in the impeller and draft tube section may be due to the increase of flow causing internal flow instability, resulting in backflow phenomenon. As an important stationary flow regions of the turbine, the hydraulic loss of the volute shows a steady growth trend with the change of flow, and the curve slope is relatively large, with a fast growth rate. At the minimum flow rate of  $177.3\text{m}^3/\text{h}$ , design flow condition of  $197\text{m}^3/\text{h}$ , and maximum flow rate of  $275.8\text{m}^3/\text{h}$  in the simulation, the corresponding hydraulic losses are 41m, 110m, and 223m respectively. The hydraulic loss of the inlet extension section accounts for a small proportion of the total hydraulic loss, indicating that the internal flow condition is good and the loss is mainly caused by the fluid viscosity. At the flow rate  $Q=177.3\text{m}^3/\text{h}$ , it has a minimum hydraulic loss of 0.1m.

### 3.3 Internal Flow Characteristics

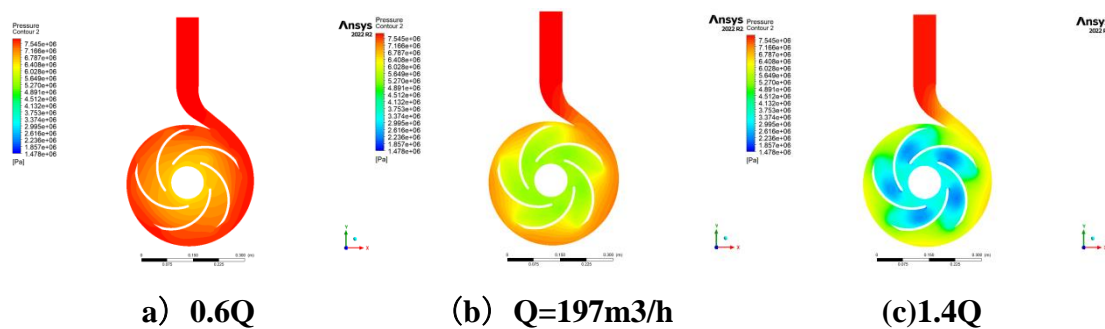


**Figure 5: Pressure Distribution at Different Flow Rates.**

To further investigate the reasons behind the changes in the external characteristic curves of the hydraulic turbine under different operating conditions, an analysis of the pressure and



velocity fields at various flow rates under stable rotational speeds was conducted. Figure 5 shows the pressure distribution on the mid-section of the hydraulic turbine under different flow conditions. Figure 5 shows that the internal pressure of the hydraulic turbine gradually decreases from the inlet extension to the impeller outlet, and as the flow rate increases, the pressure inside the volute and impeller gradually decreases. At low flow rates, it is evident that the pressure distribution at the impeller outlet is notably uneven, with the pressure at the impeller outlet being roughly 6408 kPa, whereas the pressure in the turbine's inlet extension and volute areas is significantly higher, approximately 7545 kPa. When the flow rate reaches the design conditions, the pressure distribution within the impeller improves in uniformity, but a large low-pressure area with a consistent pressure gradient forms at the impeller outlet, and an arcuate strip of high-pressure area forms at the blade inlet. The pressure in the turbine's inlet extension remains high at around 7545 kPa, but the pressure in the volute section slightly decreases to 6408 kPa, while the pressure in the impeller region drops sharply to approximately 5649 kPa. When the flow rate reaches 1.4 times the design conditions, the pressure at the impeller outlet further decreases, and a horseshoe-shaped low-pressure area forms on the suction side of the blades. The pressure at the impeller outlet is approximately 3374 kPa, while the pressure in the horseshoe-shaped low-pressure area on the vacuum side of blade is around 1857 kPa. This indicates that under high-flow conditions, the internal flow stability of the impeller is poor. Additionally, as the flow rate gradually increases, the pressure at the volute shows a decreasing trend, indicating that there is pressure loss.

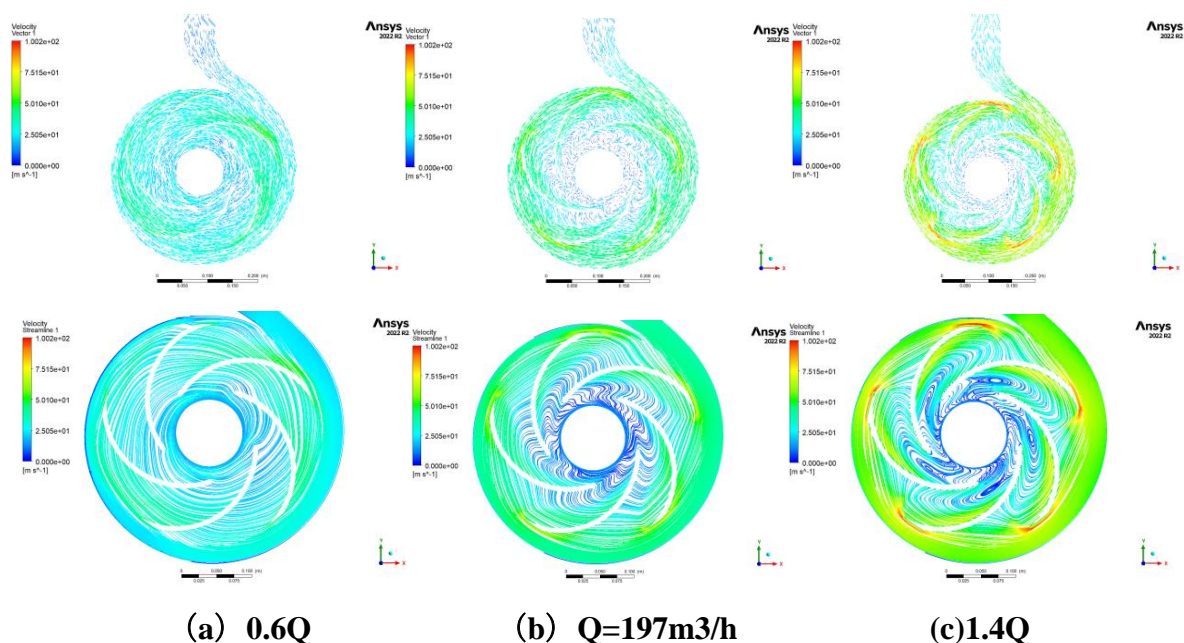
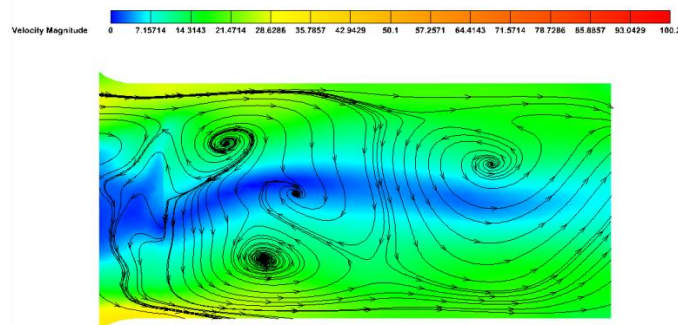
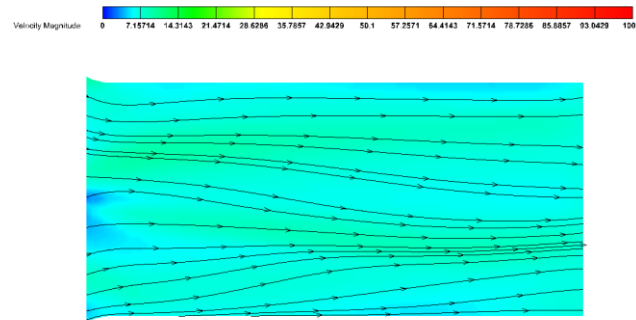
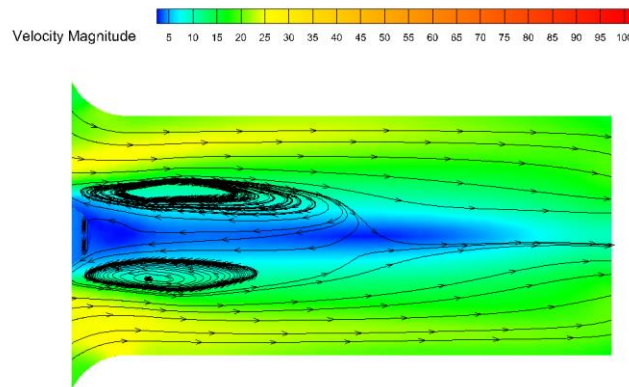


Figure 6: Velocity vector and streamline plots at different flow rates.

Figure 6 shows the velocity vector and streamline plots on the mid-section of the hydraulic turbine under different flow conditions. As shown in Figure 6, under low-flow conditions, the flow field is relatively stable with uniform streamlines in the volute and impeller channels. The internal flow velocity is approximately 25.05 m/s, but at the blade inlet, the flow velocity is relatively faster at 42 m/s. As the flow rate gradually increases, under design conditions, the velocity in the normal flow region of the impeller is about 50 m/s. Chaotic low-speed vortices are generated at the blade outlet end face. Additionally, a small, high-density high-speed vortex forms at the blade tip where the impeller connects to the volute, with a velocity of approximately 66 m/s. When the flow rate exceeds the design conditions, as shown in Figure 6(c), the velocity in the impeller area is mostly around 66 m/s. Axial low-speed vortices of various scales appear near the blade outlets in each channel, and a backflow region forms at the core of the vortex, further exacerbating energy loss and causing an increase in hydraulic losses. The flow velocity of the low-speed vortices is generally below 25.05 m/s. Additionally, the range and speed of the high-speed vortex at the connection between the impeller and the volute further expand and increase, reaching a velocity of about 100.2 m/s. The presence of high-speed vortices may have a certain impact on the stability of the internal flow field and the efficiency of energy transfer within the turbine. It is evident that when the hydraulic turbine operates normally, with its inlet and outlet flow rates slightly below the optimal values, it can effectively reduce the hydraulic losses within the impeller and improve the stability of the internal flow field.



(a)0.6Q

(b)  $Q=197\text{m}^3/\text{h}$ (c)  $1.4Q$ 

**Figure 7: Streamline distribution inside the draft tube under different operating conditions.**

Figure 7 shows the streamline distribution inside the draft tube of a hydraulic turbine under different operating conditions to investigate the changes in hydraulic losses. Under the design operating conditions, the streamlines inside the draft tube are relatively uniform, the flow is relatively stable, the hydraulic losses are small, and the flow velocity within the tube is basically stable at around 7 m/s. When the flow rate inside the draft tube deviates from the design flow conditions, in the low-flow range, the flow velocity inside the draft tube increases to 21 m/s. However, the internal flow becomes more turbulent, forming multiple small vortices. Each vortex has a different rotation direction and forms twisted, strip-shaped low-speed regions at the entrance of the draft tube, obstructing the normal flow of the liquid and interfering with the stability of the flow field. The flow velocity in these regions is less than 7 m/s. In the high-flow regime, the overall flow velocity within the draft tube is essentially the same as that under low-flow conditions, at 21 m/s. The vortices have moved to the entrance of the draft tube, and while their number has decreased to two, the range of the vortices has further expanded, with their rotation directions being exactly opposite. At the

entrance of the draft tube, a more regularly shaped conical low-speed region is formed, and its flow velocity is also less than 7 m/s. It is evident that when deviating from the optimal operating conditions, a certain backflow phenomenon occurs within the draft tube, which aligns with its hydraulic loss characteristic curve.

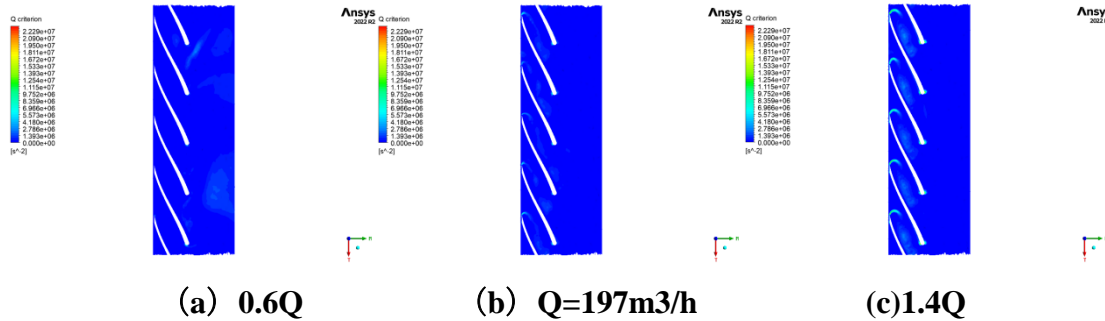
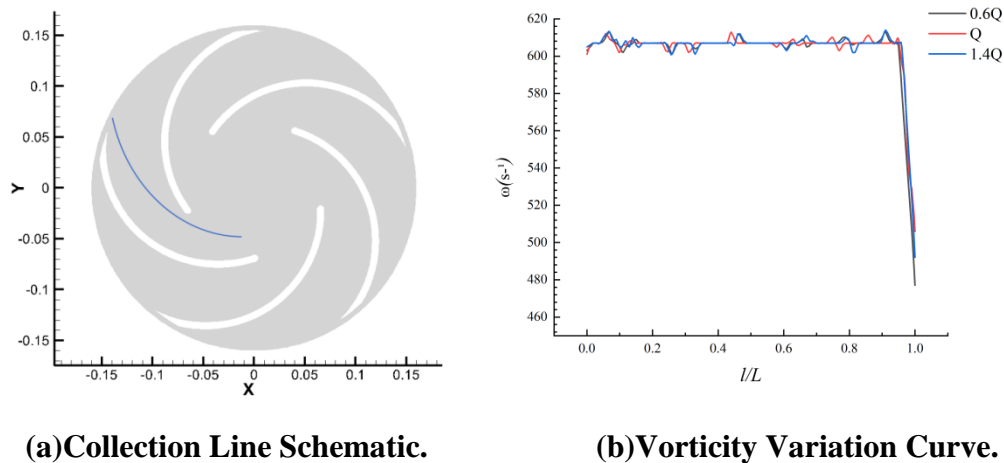


**Figure 8: Vorticity Contour of the Blade Unfolding View.**

Figure 8 shows the vorticity distribution contour of the hydraulic turbine blade unfolding view under different flow conditions. To further analyze the flow characteristics inside the impeller. As can be seen from Figure 8, under low-flow conditions, there is only a slight distribution of vorticity at the blade outlet. As the flow rate increases, under design conditions, an arc-shaped vorticity distribution forms at the blade inlet, and a point-like vorticity concentration area forms at the blade outlet. In the high-flow range, the arc-shaped vorticity distribution at the blade inlet further expands and deepens, forming a cloud-like vorticity distribution within the blade passage, and an additional vorticity concentration area appears at the blade outlet. This indicates that under low-flow conditions, the flow inside the impeller is relatively stable, with only a small amount of vorticity distribution present at the impeller outlet, which aligns with the pressure contour distribution under low-flow conditions. However, as the flow rate increases, under design and high-flow conditions, vorticity distribution begins to form around the blades and continues to increase and expand.

Figure 9 is the Variation curve of vorticity on the collection line at the middle section of the hydraulic turbine impeller under different working conditions. It can be seen from Figure 9 (a) that the blue thick line in the figure represents the collection line on the middle section of the impeller. The variation curve of vorticity on the collection line is shown in Figure 9(b). It should be noted that the abrupt changes in the three data curves in Figure (b) are due to the extension of the collection line to the volute outlet. In Figure (b), the horizontal coordinate  $l/L$  represents the relative position of the collection points on the collection line, which is the

ratio of the distance from the starting point to the collection point and the length of the collection line. The figure shows that the vorticity variation curves under different flow conditions are fluctuating at  $607s^{-1}$ , and there is a certain similarity in the variation patterns of the vorticity curves under different flow rates. However, at the exit of the impeller, the frequency of change in the vorticity curve under high flow rate is significantly higher than other conditions, indicating more unstable liquid flow.



(a) Collection Line Schematic.

(b) Vorticity Variation Curve.

**Figure 9: Vorticity Variation Curve on the Collection Line of the Impeller's Middle Section.**

#### 4 CONCLUSIONS

This study utilizes fluid mechanics methods to conduct a numerical simulation of the external characteristics, internal flow field evolution, and changes in hydraulic losses of a single-stage cantilevered hydraulic turbine with a specific speed of 23.1. The results show that the total hydraulic loss of the hydraulic turbine decreases first and then increases. In the high-flow range, the total hydraulic loss increases rapidly. The variation of water power loss in impeller is complex. The hydraulic loss within the volute gradually increases with the rise in flow rate. The hydraulic losses in the inlet extension and the draft tube are relatively small. Affected by the different inlet flow, the change of internal flow field in impeller will gradually form low-speed vortex at the exit of impeller and lead to backflow phenomenon with the increase of flow. A high-speed vortex forms at the inlet of the impeller, affecting the stability of the flow field. Within the draft tube, the flow is most stable under design conditions. However, when the flow rate deviates from the design conditions, vortices form throughout the passage, leading to backflow phenomena. The variation pattern of the vorticity curves within the impeller under different flow rates exhibits certain similarities, but the fluctuation frequency

of the vorticity curve at the impeller outlet under high flow rate conditions significantly increases.

#### **ACKNOWLEDGEMENT**

The research was financially supported by the national college students science and technology innovation project (No.202411488043).

#### **REFERENCES**

1. Doshi A, Channiwala S, Singh P. Inlet impeller rounding in pumps as turbines: An experimental study to investigate the relative effects of blade and shroud rounding[J]. *Experimental Thermal and Fluid Science*, 2017; 82:333-348.
2. Shahram D, Bijan M, Ahmad N. Efficiency Improvement of Centrifugal Reverse Pumps[J]. *Journal of Fluids Engineering*, 2009; 131(2).
3. Li W, Zhang Y. Numerical simulation of cavitating flow in a centrifugal pump as turbine[J]. *Proceedings of the Institution of Mechanical Engineers, Part E: Journal of Process Mechanical Engineering*, 2018; 232(2): 135-154.
4. Li W. Effects of viscosity on turbine mode performance and flow of a low specific speed centrifugal pump[J]. *Applied Mathematical Modelling*, 2016; 40(2): 904-926.